Research article

Optimizing the topology of convolutional neural network (CNN) and artificial neural network (ANN) for brain tumor diagnosis (BTD) through MRIs

Jianhong Ye [a], Zhiyong Zhao [b], Ehsan Ghafourian [c], AmirReza Tajally [d], Hamzah Ali Alkhazaleh [e], Sangkeum Lee [f,*]

[a] *Head and Neck Surgery, The First Hospital of Jiaxing, Jiaxing, 314500, Zhejiang, China*
[b] *School of Engineering, Cardiff University, Cardiff, CF24 3TF, UK*
[c] *Department of Computer Science, Iowa State University, Ames, IA, USA*
[d] *School of Industrial Engineering, College of Engineering, University of Tehran, Tehran, Iran*
[e] *College of Engineering and IT, University of Dubai, Academic City, 14143, Dubai, United Arab Emirates*
[f] *Department of Computer Engineering, Hanbat National University, Daejeon, 34158, South Korea*

ARTICLE INFO

ABSTRACT

The use of MRI analysis for BTD and tumor type detection has considerable importance within the domain of machine vision. Numerous methodologies have been proposed to address this issue, and significant progress has been achieved in this domain via the use of deep learning (DL) approaches. While the majority of offered approaches using artificial neural networks (ANNs) and deep neural networks (DNNs) demonstrate satisfactory performance in Bayesian Tree Descent (BTD), none of these research studies can ensure the optimality of the employed learning model structure. Put simply, there is room for improvement in the efficiency of these learning models in BTD. This research introduces a novel approach for optimizing the configuration of Convolutional Neural Networks (CNNs) and Artificial Neural Networks (ANNs) to address the BTD issue. The suggested approach employs Convolutional Neural Networks (CNN) for the purpose of segmenting brain MRIs. The model's configurable hyper-parameters are tuned using a genetic algorithm (GA). The Multi-Linear Principal Component Analysis (MPCA) is used to decrease the dimensionality of the segmented features in the pictures after they have been segmented. Ultimately, the segmentation procedure is executed using an Artificial Neural Network (ANN). In this artificial neural network (ANN), the genetic algorithm (GA) sets the ideal number of neurons in the hidden layer and the appropriate weight vector. The effectiveness of the suggested approach was assessed by utilizing the BRATS2014 and BTD20 databases. The results indicate that the proposed method can classify samples from these two databases with an average accuracy of 98.6 % and 99.1 %, respectively, which represents an accuracy improvement of at least 1.1 % over the preceding methods.

1. Introduction

The brain, which regulates the functioning of the human body and the nervous system, can be regarded as the primary organ of the body. Any complications that arise within this organ have the potential to significantly impact an individual's existence. Brain tumors (BTs), which manifest as dense tissue within the brain, are among the most frequent complications associated with the brain [1]. Early detection of a BT, whether benign or malignant, is critical for preserving a patient's life. Utilizing BTD with common instruments is difficult for a number of factors. One contributing factor is the intricate structure of the brain, which renders numerous functional aspects of this organ enigmatic even to specialists. A second factor is that clinical examinations of BTD are complicated by the skull's encirclement of the brain; therefore, BT is diagnosed using Magnetic Resonance Imaging (MRI) to analyze the brain's structure [2]. In addition to specialized knowledge, identifying the type of tumor from brain images is a complex undertaking that demands experience and high levels of precision [3]. As a consequence, technical difficulties, fatigue, and insufficient expertise may contribute to diagnostic inaccuracies. As a result of the aforementioned circumstances, machine vision and image analysis techniques have been implemented to address this issue; thus far, numerous studies have developed effective approaches for automatic BTD in MRIs [4]. ANNs and deep learning models have demonstrated a notable advantage over alternative machine learning approaches. To date, substantial progress has been observed in the utilization of these methodologies [5]. While the aforementioned techniques may be regarded as dependable methods in BTD, there appears to be room for improvement in their functionality with regard to precision of diagnosis, speed of processing, and simplicity of structure.

This research endeavors to fulfill the prerequisite of optimizing the configuration of neural learning models in accordance with the attributes of the BTD problem. An endeavor has been undertaken in this article to enhance the performance of ANNs and CNNs when addressing the issue of BTD through the utilization of GA to optimize their configuration. The aforementioned issue is subdivided into the subproblems of image segmentation and image feature classification in order to achieve this objective. The first sub-problem is resolved utilizing a CNN, while the second is resolved utilizing an ANN. The GA is utilized in the proposed method to ascertain the optimal configuration for these two models. A concise summary of the contribution of this paper can be derived from the afore-mentioned explanations:

- An effective method for optimizing the configuration of a Convolutional Neural Network (CNN) for the segmentation of brain MRIs is introduced in this article. Ensuring optimal image segmentation quality, this CNN's adjustable hyper-parameters are determined utilizing GA and are based on an encoder-decoder architecture.
- A solution for classifying the characteristics of MRIs by combining ANN and GA is presented in this paper. GA concurrently performs the configuration and training of NN in this combined classifier. Thus, the configuration of every chromosome within this convolutional neural network simultaneously determines the quantity of hidden layer neurons and the weight vector of the NN.

These two cases, which, to the authors' knowledge, have not been previously investigated in MRI-based research on BTD, can be regarded as novel contributions of the current paper that resolve a lacuna in the literature. The subsequent sections are structured as follows: In section 2, the investigation records are examined. The proposed methodology is delineated in Section 3, while the research findings are examined and discussed in Section 4. Section 5 concludes with a summary of the research findings.

2. Literature review

The research endeavors undertaken in the domain of MRI processing and BT can be broadly classified into two categories: BT segmentation and classification of tumor types. A method for BTD based on deep learning was described in Ref. [6]. This approach commences by extracting three distinct categories of features from the input images. The initial two classifications are predicated on feature extraction methodologies, whereas the third classification of features is derived via a CNN. By employing optimization techniques, the most favorable features are then chosen from among these three sets. Following this, the chosen features are identified and categorized utilizing a support vector machine (SVM). The approach for BTD, as described in Ref. [7], integrated the Whale Harris Hawks Optimization (WHHO) algorithm with a CNN model.

A secure blockchain-based framework for BTD was suggested in Ref. [8]. This approach comprises three primary stages. To assure data security, MRI images are encrypted and decrypted using the SHA-256 algorithm in the initial step. Subsequently, the decoded images are transmitted to the Javaria (J), a two-qubit quantum model that classifies tumors using three layers—two dense layers and one SoftMax layer. The categorized tumor images are subsequently transmitted to a semantic segmentation model. A novel framework for the categorization of BTs was presented in Ref. [9]. Pre-processing, segmentation, feature description, feature selection, and classification are all components of this framework. The feature set comprises the co-occurrence matrix (COM), run length matrix (RLM), and gradient features extracted from segmented images, which are employed to describe the feature. Then, nine features are selected from this set and utilized as input for four classification models.

A BT classification utilizing deep learning techniques was introduced in Ref. [10], which incorporates an enhanced CNN created by integrating transfer learning and data augmentation methods; however, there is no significant improvement when compared to other methods. The Kernel SVM (KSVM) model was utilized in Ref. [11] to classify and diagnose BTs in MRIs. The process commences by applying the Normalized Median Filter (NMF) to eliminate image distortion and enhance the overall quality of the image. Following the segmentation of the input image with a double threshold in the second phase, the image features are described using a combination of the Spatial Gray Level Dependence Matrix (SGLDM) and the Gray Level Co-occurrence Matrix (GLCM). The feature selection process is executed using the Harris Hawks Optimization (HHO) algorithm in the third phase. The chosen attributes are subsequently

categorized utilizing the KSVM model.

An Internet of Things (IoT)-based computational model for BTD in MRIs was presented in Ref. [12] utilizing deep learning techniques. This approach involves the integration of a CNN model and a Long Short-Term Memory (LSTM) model. By employing this combination, CNN's ability to extract image features utilizing LSTM would be enhanced. The results of this study demonstrated that the aforementioned combination outperforms the fundamental CNN model when applied to classification tasks. A comparable approach, which combined CNN and LSTM, was implemented in Ref. [13] to categorize BTs in MRIs. In this learning model, a time distribution function encircles each layer. This approach employs time-dependent data to diagnose tumors through the utilization of a quadruple sequence of magnetic resonance imaging (MRI) images for every individual patient. A method for segmenting 2D brain tumors in MRI images utilizing deep neural networks and data augmentation techniques was proposed in Ref. [14]. This technique employs a Deep Neural Network (DNN) model that is constructed using encoder-decoder architectures and data amplification. By extending the inherent similarities among tens of thousands of synthetic images from a restricted set of BTs identified by specialists, the data augmentation solution enables the DNN to acquire more comprehensive knowledge.

An approach utilizing deep learning was proposed in Ref. [15] for the identification of tumor regions in MRI images. Before proceeding with this technique, the input images are preprocessed to enhance their quality. Following this, the salient features of the images are extracted using two trained DNNs and merged using the partial least squares (PLS) method. Agglomerative clustering is subsequently implemented to pinpoint the location of the tumor. An improvement in the classification accuracy of brain tumor categories was achieved through the implementation of machine learning techniques [16]. The performances of nine distinct classifications were contrasted. This investigation employed MRIs in conjunction with a set of clinical data. Random Forest has the maximum classification accuracy (87.5 %) among the nine algorithms that were evaluated; however, it is not yet on par with other algorithms of a similar nature.

Several studies have investigated the use of deep learning to classify brain tumors from MRI scans. A CNN-based model from Ref. [17] demonstrated its diagnostic potential by increasing neuroradiologist accuracy by 12.0 %. An alternative approach ([18]) that integrated a two-dimensional convolutional neural network (CNN) and an auto-encoder network demonstrated an average accuracy of 96.47 % when used to classify three distinct categories of tumors. The network's simplicity further supports its potential for clinical application.

Utilizing Bayesian Optimization, the hyperparameters of a CNN model were optimized by the authors of [19], resulting in a minimum 1.62 percent enhancement in diagnostic accuracy. In the interim, a YOLOv7 model was refined through transfer learning in Ref. [20], resulting in a 0.7 % improvement in its capability to detect diverse brain lesions.

A deep-learning model known as DLBTDC-MRI was developed by researchers [21] to automate the detection and classification of brain tumors. A final classifier is employed for diagnosis, following adaptive fuzzy filtering for preprocessing and chicken swarm optimization for segmentation and feature extraction, respectively.

In conclusion [22], introduced a method for ensemble learning. The model utilizes Singular Value Decomposition to reduce dimensionality, Social Spider Optimization for segmentation, and a composite classifier that integrates the Naïve Bayes, SVM, and K-Nearest Neighbor algorithms.
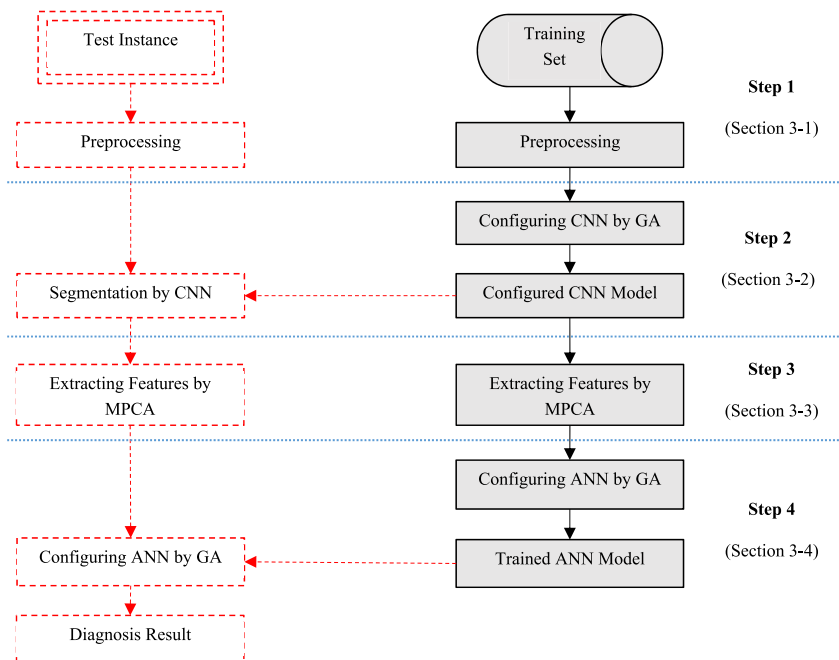

Fig. 1. Steps of the proposed method.

3. Proposed method

The majority of MRI-based BTD methods consist of the subsequent stages: image pre-processing, feature extraction, and diagnosis. Additionally, segmentation techniques can be utilized to decrease the problem's complexity. Each of the aforementioned stages is critical, and the ultimate efficacy of the system can be significantly impacted by the technique employed. The procedure for detecting brain tumors as proposed is illustrated in Fig. 1. As illustrated in the figure, the proposed methodology comprises the subsequent stages:

1 Preprocessing of the images
2 Image segmentation based on CNN and GA
3 Feature extraction based on MPCA
4 Classification of features based on ANN and GA

The procedures pertaining to the training phase are depicted on the right-hand side of Fig. 1, while those pertaining to the testing phase are illustrated on the left-hand side. Each training and testing phase stage of the proposed method is also delineated in this diagram. The pre-processing of the input images commences the training portion of the proposed method, as depicted in the diagram. Preprocessing is implemented with the objective of distinguishing the brain region from the background in the input image. Then, in the second phase, GA is used to determine the optimal CNN configuration for image segmentation; during this process, hyper-parameters that can be adjusted in each layer of the CNN in question are determined so as to maximize the quality of segmentation. In order to segment training images, the configured NN model is applied. The MPCA algorithm is employed to extract the reduced feature set from the segmented images subsequent to the segmentation process. The aforementioned characteristics are fed into an ANN in order to execute BTD during the fourth stage of the suggested approach. Thus, an ANN is configured using GA in the final phase, while the optimal weight vector for its neurons is simultaneously determined. This NN is subsequently implemented to identify the malignancy in the test samples. The remainder of this section elaborates on each phase of the proposed method.

3.1. Image preprocessing

The proposed method begins with the pre-processing of MRIs, which consists of removing redundant information and improving the quality of the images. To achieve this objective, the input image is processed as follows: initial identification of the brain region, followed by enhancement of its contrast using the Histogram Equalization (HE) method [23]. Every individual segment of the MRI is denoted as $I_{(w \times H)}$. The grayscale image segment in question comprises two overarching components: the cerebral region and the background of the image. As the initial stage in the pre-processing phase, these regions are isolated from one another. According to the investigations, the maximal luminance intensity of the background region in each segment of the MRI images using the gray color system (ranging from 0 to 255) is 13.

Image I is initially converted to binary format utilizing threshold 14. This causes a portion of the brain's internal regions and the pixels comprising the background region to receive the value 0, while all other regions receive the value 1. The resulting binary image is defined as $B_{w \times H}$. The subsequent steps involve the extraction of all connected regions present in the image, with the identification of the greatest connected region in image B determined by the count of its member pixels. The connected region that has been chosen represents an approximation of the brain. In order to enhance the margins of this region in binary image B, the erosion operator is implemented. When the erosion operator's structural element is specified as X, the erosion operator can be mathematically represented as Equation (1) [24]:

$$B \ominus X = \{z | (\widehat{X})_z \in B\} \tag{1}$$

Each eroded element z is only considered when the structural element X is a subset of the binary image B, as expressed by the preceding relationship. The proposed method conceptualizes structural element X as a three-radius circle. The eroded image is represented as Z. The image depicts a region of the brain denoted by the binary value 1, while certain internal regions of the brain tissue, characterized by a luminance intensity below the threshold of 13, are denoted by the value 0. As a result of the brain region's integrity, all the empty spaces in image Z are subsequently filled with 1. This is accomplished by populating all connected subregions containing 0 values surrounded by 1 values with the value 1. A binary mask of the brain region is the outcome of this work; it can be utilized to distinguish brain tissue from the background in primary image I.

$$J = Z \times I \tag{2}$$

By applying Equation (2) to the entire background pixels of image I, the result is 0. Subsequently, the brain region is isolated from the image by reducing the box that encloses the range of non-zero values. The HE technique is employed to enhance the image of the brain region as the pre-processing phase progresses [23]. The image obtained is utilized as the input for the method's second phase.

3.2. Image segmentation based on CNN and GA

In order to segment the images, the preprocessed images serve as the input for the second stage of the proposed method. A CNN that has been optimized by GA is employed for this objective. The CNN model utilized in the proposed method is a CNN with a coding-

decoding architecture; its dimensions (length and breadth), the number of filters in each convolution layer, and the type of pooling functions are all configurable hyper-parameters. The configurable parameters of this NN are thus defined as a set of optimization parameters, and the optimal combination of these hyper-parameters is determined using GA. A flowchart illustrating the automatic CNN configuration procedure for image segmentation in the proposed method is presented in Fig. 2.

As illustrated in Fig. 2, the segmentation phase of the suggested methodology commences with the preliminary configuration of the optimization model parameters within the problem domain. Each hyperparameter that is configurable in the CNN model is designated as an optimization parameter during this stage, and its respective allowable limits are established. GA subsequently produces response vectors for the initial population. This operation is performed at random and in accordance with the limits specified for each hyperparameter in the preceding phase. A new CNN model is generated by applying the possible configurations specified by each chromosome in GA to the existing CNN model. Thus, a distinct CNN model is constructed for each chromosome in the population; this model is trained using a limited dataset. The fitness of each chromosome is assessed in this instance by utilizing the DICE criterion and the segmentation quality of the corresponding CNN model. The termination conditions are then evaluated, and if the algorithm continues, selection, crossover, and mutation operators are used to generate a new population. This procedure is iterated until one of the termination conditions is fulfilled, at the very least. The following are the conditions for termination of GA:

- The number of generations reaches the threshold G.
- The best fitness discovered does not improve after T consecutive iterations.
- The fitness criterion is maximized.

Following a description of the proposed CNN model's general structure for image segmentation in the remainder of this section, the GA optimization procedure for the model is presented. Encoder-decoder structure forms the foundation of the proposed CNN model for MRI image segmentation. It consists of two coding and decoding sections that occur consecutively and concludes with a Softmax layer. The encoding and decoding components of this paradigm are comprised of two dense layers. The architectural design is illustrated in Fig. 3.

The proposed CNN structure consists of two consecutive dense layers in its coding section, separated by a pooling layer, as depicted in the figure. In the coding section of the CNN model under consideration, MRI features are encoded. Decoding section-encoded features are utilized to reconstruct the segmented image. Although the configuration of the dense layers in the decoding section resembles that of the coding section, these layers may not possess identical properties. The CNN model's image segmentation output is produced by a convolution and Softmax layer that follows the conclusion of the decoding section.

Fig. 4 illustrates the configuration of every dense layer within the CNN model that has been proposed. According to the diagram, each dense layer in the proposed CNN model is composed of four consecutive layers that receive input data. Every individual layer comprises three convolutions, normalization, and activation operators. In each convolution layer, the dimensions of the filter, including its length, breadth, and size, are optimized using GA.
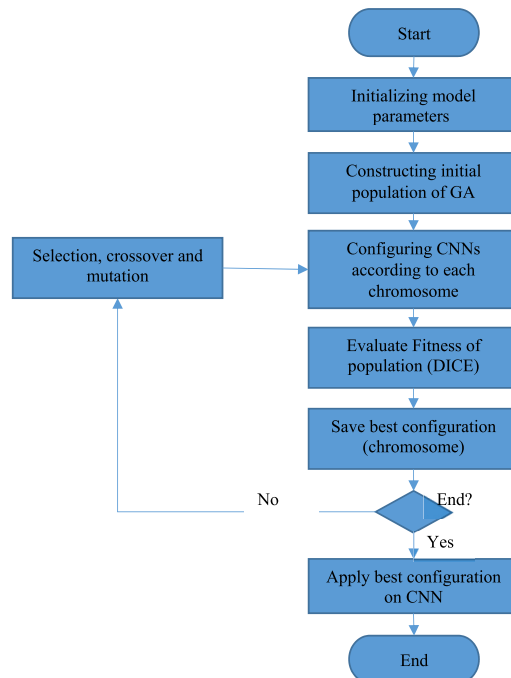

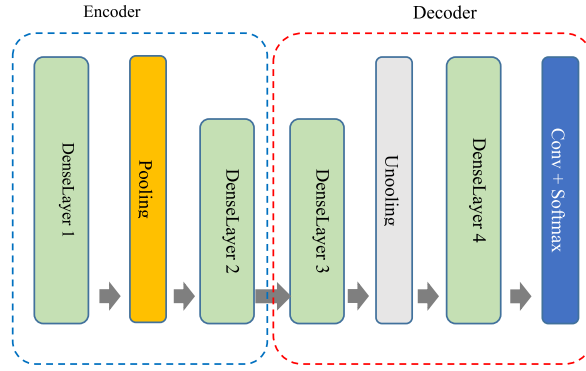**Fig. 2.** CNN automatic configuration process in the proposed method.

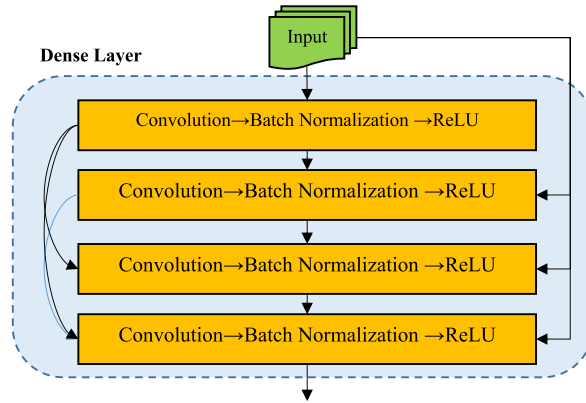**Fig. 3.** Structure of the proposed CNN model based on dense layers.

Fig. 4. Architecture of dense layers in the proposed CNN model.

The subsequent section describes how GA ascertains the optimal configuration for this CNN model. As previously stated, every configurable hyperparameter is regarded as an optimization variable in the proposed CNN model. The following parameters comprise them:

- filter breadth, length, and size in each convolution layer between dense layers 1 and 4. Given that each dense layer comprises four convolution layers, this category corresponds to a total of 48 optimization parameters ($3 \times 4 \times 4$).
- The pooling function type, which may be maximum or average. As a result of the aggregating layer incorporated into the proposed CNN model, there are precisely one optimization variable of this sort.
- filter number, filter length, and filter breadth in the final convolution layer of the proposed CNN model, which follows the decoding section. Consequently, three optimization parameters pertain to this category.

As a result, there are 52 adjustable parameters (or optimization variables in GA). In the CNN configuration problem, the length of each chromosome is thus specified as a 52-element numeric vector. The hyperparameters of $1 + 16$ convolution layers are regulated by 51 genes located on each chromosome. Among these genes, 17 variables are associated with the number of filters in each convolution layer and can take on the values 8, 16, 32, 64. Additionally, the breadth and length of the convolution filters are determined by 17 variables, each of which can take on one of the following values: 3,4,5,6,7. The final variable in the chromosome structure designates the Pooling function type, with values of 0 (maximum) or 1 (average).The fitness function for each chromosome, taking into account the structure described above, is delineated below. In order to assess the fitness of individual chromosomes, the CNN model is initially fitted with the configuration ascertained by it. Following this, segmentation and training are performed on a subset of preprocessed images. The fitness criterion DICE is applied to the segmented images of this dataset in order to assess their quality [25].

$$DICE = \frac{1}{N} \sum_{i=1}^{N} \frac{2|S_i \cap T_i|}{|S_i|+|T_i|} \tag{3}$$

N is denoted as the quantity of images in Equation (3). Furthermore, the segmentation output and background segmentation for image i are denoted by S_i and T_i, respectively. The function $|.|$ returns the set's capacity. At this stage of the proposed method, the aim of GA is to determine a CNN configuration that maximizes the fitness function specified in Equation (3). Taking into account the fitness

function and the described structure for each chromosome, the following GA stages are utilized to optimize the configuration of the CNN model:

Algorithm 1: Optimization of CNN model based on GA

1 The proposed approach generates an initial population of chromosomes in which each chromosome specifies the values of the CNN model's hyperparameters, which are determined according to the contents described in this section.

2 Evaluation of the Fitness of Population Chromosomes: During this phase, a CNN model is constructed by utilizing the parameters of individual chromosomes. Subsequently, the model is trained using a limited dataset, and the fitness is assessed using Equation (3).

3 Parent selection: The Roulette Random Wheelchair Algorithm is utilized in this stage to ascertain the parent chromosomes.

4 Recombination: Each pair of parent chromosomes is recombined into two offspring chromosomes via two-point crossover in Step Four.

5 Mutation Analysis: Following the generation of each child's chromosome, an assessment is conducted to determine whether a mutation is probable, using a threshold of 0.02. Should a mutation occur, one of the chromosome genes (or one of the CNN model hyperparameters) is substituted with the parameter, which has a random value within the corresponding interval, and fitness is subsequently computed for that particular chromosome.

6 The optimal chromosomes are transmitted to the subsequent generation after being sorted according to their fitness.

7 The fitness value is modified for the optimal chromosome from the initial generation.

8 The algorithm terminates if the termination condition is satisfied; otherwise, it iterates back to step 3.

This phase yields an optimal CNN model capable of performing MRI segmentation that is most similar to the background segmentation. All images are segmented using this CNN model in preparation for the feature extraction that follows.

3.3. Feature extraction based on MPCA

In the third step, the proposed method applies MPCA to extract the features of segmented MRIs. For this objective, consider a database consisting of N -segmented images, the dimensions of each sample are r $\times$ s. Each sample can be defined as $M_{R \times S}$, and the entire database can be defined as $\mathscr{R}_{R \times S \times N}$.

Applying $\mathscr{R}$ in the MPCA algorithm, the extracted features matrix for $\mathscr{R}$ is $D_{N \times P}$ in which $P \leq \max(R, S)$. As such, the $R \times S$ features of every sample reduce to P features, and each row of Matrix D is the representative of the sample corresponding to it in the database $\mathscr{R}$. The feature extraction process is displayed in Fig. 5.

The following is a computational process to extract the feature applying MPCA algorithm. MPCA is obtained as a multilinear equation of PCA. Assuming a set of tensor training samples $\{x_i, i = 1, 2, ..., n\}$, MPCA defines a multilinear map $\{U_l \in \mathbb{R}^{I_l \times P_l}, l = 1, 2, ..., n\}$, L = 1, 2, ..., n$\}$ mapping the main tensor space $\mathbb{R}^{I_1 \times I_2 \times ... \times I_N}$ to the tensor space $\mathbb{R}^{P_1 \times P_2 \times ... \times P_N}$ with $P_l < I_l, l = 1, 2, ..., N$.

Where, $y_i = x_i \times_1 U_1^T \times_2 U_2^T ... \times_N U_N^T, i = 1, 2, ..., n$ are derivated so that most of the variances seen between the main tensor sample are obtained. The value of this total tensor variance is defined as follows [26]:

$$S_T = \sum_{i=1}^{n} \left\| y_i - M_y \right\|^2 \tag{4}$$

$$\{U_l, l = 1, 2, ..., N\} = \underset{U_l^T U_l = I}{\mathrm{argmax}} S_T \tag{5}$$

In Equations (4) and (5), M_y is the mean tensor provided by $M_y = (1/n) \sum_{i=1}^{n} y_i$. The matrices $U_l \in \mathbb{R}^{I_l \times P_l}, l = 1, 2, ..., N$ maximizing the total tensor variance S_T, are obtained by solving the optimization problem [26].

Since there is no known optimal solution for the optimization problem of (5), it is assumed that $\widetilde{x} \in \mathbb{R}^{I_1 \times I_2 \times ... \times I_N}$ is a test tensor (new). The lower dimension tensor obtained via MPCA $\widetilde{y} = \widetilde{} \times_1 U_1^T \times_2 U_2^T \times_3 ... \times_N U_N^T$ can be used for display or classification instead of $\widetilde{x}$. For the purposes of feature extraction and image description, this method is more efficient when the horizontal and vertical correlation of the data are considered simultaneously. The attributes that are obtained in this stage serve as input for the subsequent phase of classification.
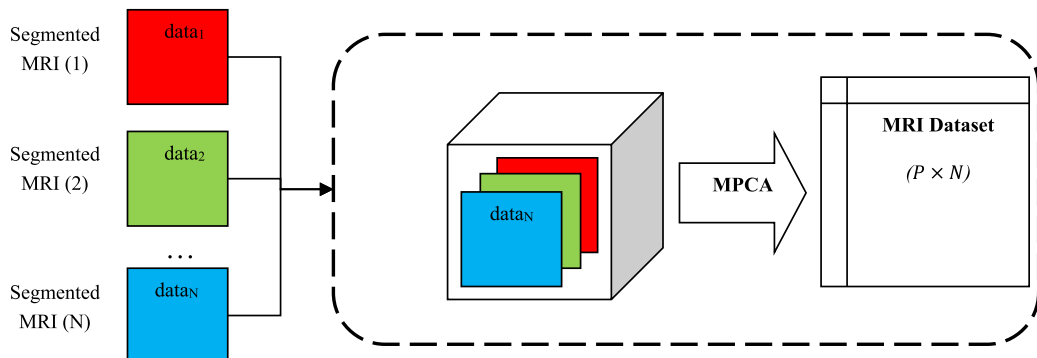

Fig. 5. Feature extraction process using MPCA algorithm.

3.4. Classification of features based on ANN and GA

The final stage of the suggested approach involves the classification of the extracted features using an ANN. The procedure of identifying the most effective configuration for the ANN is a laborious one. Conversely, conventional training functions utilized in NN training do not provide an assurance of attaining optimal NN performance in sample classification. As a consequence, GA is employed in this stage to resolve these two issues. GA thus simultaneously determines the optimal number of hidden neurons to be included in the NN and establishes the weight vector for said neurons. Fig. 6 illustrates the general NN model utilized in the proposed method for feature classification. Classifying features is accomplished using a NN with a concealed layer, as shown in Fig. 6. The output layer of this NN comprises the number of target classes in the problem, while the number of input neurons is equivalent to the number of features extracted via the MPCA algorithm. A logarithmic sigmoid characterizes the network's transfer function. GA determines the number of hidden layer neurons, the weight vector between neurons, and the NN biases in this ANN model. The process outlined in the second phase of the proposed method (algorithm 1) is also mirrored in this step of the GA optimization mechanism; chromosome structure and various fitness functions of ANN optimization are utilized in this step. Explanations for these items can be found in the subsequent section.

The length of the weight vector of the NN is dependent on the number of neurons in the hidden layer, which is determined by each chromosome during the optimization step of the ANN model. Consequently, the length of the chromosome population in this stage of the proposed method is variable. Given Equation (6), the length of each chromosome can be calculated in this instance.

$$L = 1 + (H \times (I+1) + P \times (H+1)) \tag{6}$$

In the given context, I denotes the input layer's neuron count, H represents the concealed layer's neuron count, and P signifies the output layer's neuron count. The number of neurons in the hidden layer of the ANN model is specified by the first gene on each chromosome, as indicated in Equation (6). This value is expressed as an integer in Refs. [5,15]. $H \times (I+1)$ of the next genes in every chromosome is assigned to identify the weight between the neurons of the input layer and the hidden layer. At last, $P \times (H+1)$ of the last gene in each chromosome identify the weight between the hidden layer and the output layer. That these weight values are determined as a real number in [-1, +1].

In order to assess the fitness of each chromosome described in the genetic population, an ANN model is initially constructed using the chromosome-determined weight vector values and the quantity of neurons. After applying the training samples to the input layer of the ANN model, the output of this learning model for each individual sample is determined. The fitness of that particular chromosome can be assessed by comparing the output of the ANN model to the actual outputs of the training samples.

$$Fitness = \frac{T}{N} \tag{7}$$

In Equation (7), N denotes the total number of training samples and T signifies the number of training samples for which the output of the ANN model is identical to the actual output. At this stage of the proposed method, the objective of the GA is to determine an ANN configuration that maximizes the fitness function in Equation (7). Once this ANN model has been established, it is implemented to categorize novel samples and diagnose brain lesions.

4. Results

The efficacy of the proposed method was assessed through its implementation using MATLAB 2016a software. The experiments aimed to assess the efficacy of the proposed method with respect to the precision and caliber of brain tumor classification. The outcomes of these evaluations were then compared to those of prior studies that pursued similar objectives. Furthermore, the input for the
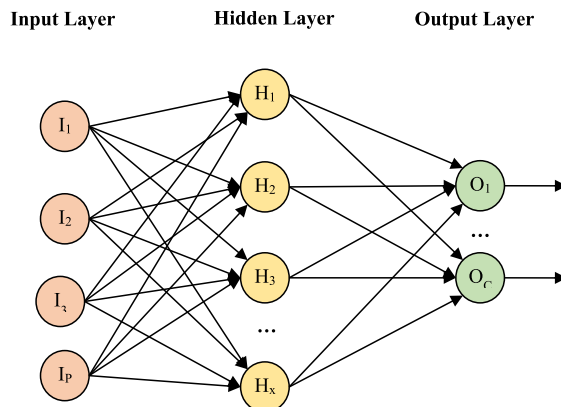

Fig. 6. ANN model for feature classification.

experiments consisted of MRI images that were accessible through the databases BRATS2014 [27] and BTD20 [28]. After describing the specifications of the databases in question, an analysis of the results obtained is provided. There are 3000 brain MRI images in BTD20, 1500 of which contain brain lesions and 1500 of which do not. Experimentally, each and every image from this database was implemented. Conversely, when evaluating the efficacy of the proposed method using BRATS2014 samples, a subset of 500 was utilized, consisting of 250 samples without tumors and 250 samples with tumors. The database images in both of these collections were resized to 250×250 pixels. It is important to mention that for every MRI image contained in these databases, a single image slice was utilized.

As mentioned in the preceding section, GA was implemented to refine the CNN model's configuration. The population size and number of generations of the GA are established as 50 and 300, respectively, in this instance. Additionally, each chromosome has a recombination rate of 0.8 and a mutation rate of 0.02. Additionally, a maximum of 100 unchanged iterations is permitted. Furthermore, a fitness test was conducted for each chromosome, employing 10 % of the database samples and utilizing the DICE criteria. Fig. 7 illustrates the fitness variations of genetic algorithms on a graph.

According to the data presented in Fig. 7, the GA achieved the optimal configuration for the CNN model with a fitness value of 0.96115 after 161 iterations. The presented graph illustrates how the genetic algorithm iterated in an effort to optimize the CNN model's configuration. As the number of generations of the optimization algorithm increases, the chromosome population is concurrently pushed in the direction of the global optimum. This demonstrates that the proposed algorithm effectively determines the optimal CNN model configuration. Fig. 8 illustrates an instance of segmented images produced by the optimal CNN model. The image segmentation is illustrated in this figure along the axial and coronal axes. The figure presents the initial image, the segmentation result, and the ground-truth segmentation in Fig. 8a, b, and 8c, respectively. Furthermore, a comparison is made between two identical regions of the segmented image and the background image in Fig. 8d. This figure demonstrates that the CNN model under consideration can accurately segment images.

The investigations employed the cross-validation method with a total of ten iterations. During each iteration, ninety samples were utilized to train the learning models, while the remaining ten percent were set aside for testing purposes. Furthermore, a distinct evaluation approach was conducted for both BRATS2014 and BTD20. During ten iterations of cross-validation, Fig. 9a and b illustrate the accuracy of the proposed method in comparison to alternative methods for classifying BRATS2014 and BTD20 images, respectively.

The graphs presented herein illustrate a comparison between the performance of the proposed method and that of alternative learning models employed for classification. The CNN + ANN state denotes the circumstance in which the proposed procedure for optimizing the CNN and ANN models does not employ GA. By comparing the proposed method to this state, the efficacy of the GA in optimizing the learning models utilized by the proposed method can be determined. Additionally, the term "state" pertains to the situation in which the SVM classifier is employed for BTD rather than the suggested ANN model. The kernel function of the SVM model utilized in the comparisons is linear. Furthermore, the approach that has been suggested has been assessed in comparison to DACBT [10] and the model that Rammurthy et al. [7] introduced.

The proposed method exhibits enhanced accuracy in classifying the brain tumor across all iterations, as demonstrated in Fig. 9. Furthermore, the proposed strategy enables the attainment of a higher average accuracy when compared to alternative methods. Given that the sole distinction between the contrasted methods is the classification technique employed, the accuracy enhancement achieved by the proposed method can be ascribed to the classification model's suitable performance. The proposed approach employs a genetic algorithm in conjunction with an ANN to classify brain tumors. The tumor in BRATS2014 and BTD20 can be accurately identified by this combination with respective average accuracies of 99.1 % and 98.6 %. Possible cause for the increased precision of the suggested approach in BTD20: variation in the quantity of training samples. Due to the fact that the number of samples in BTD20 is six times that of the BRATS2014 database, the proposed model can utilize more training samples to obtain a more comprehensive comprehension of the classification problem. A comparison is made between the average accuracy values of the proposed method and alternative methods for the databases BRATS2014 and BTD20, as shown in Fig. 10.

The accuracy of BTD is enhanced by the proposed method for both BRATS2014 and BTD20, as shown in Fig. 10. As previously
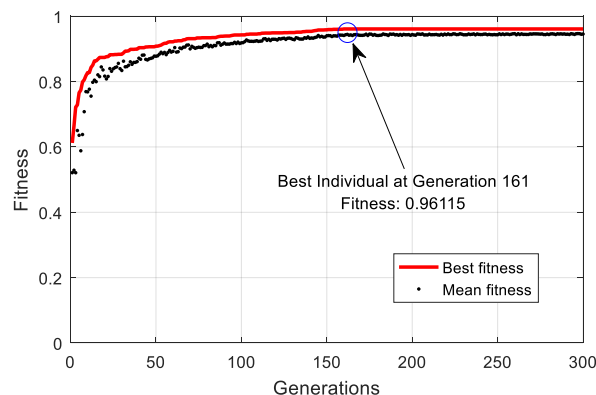

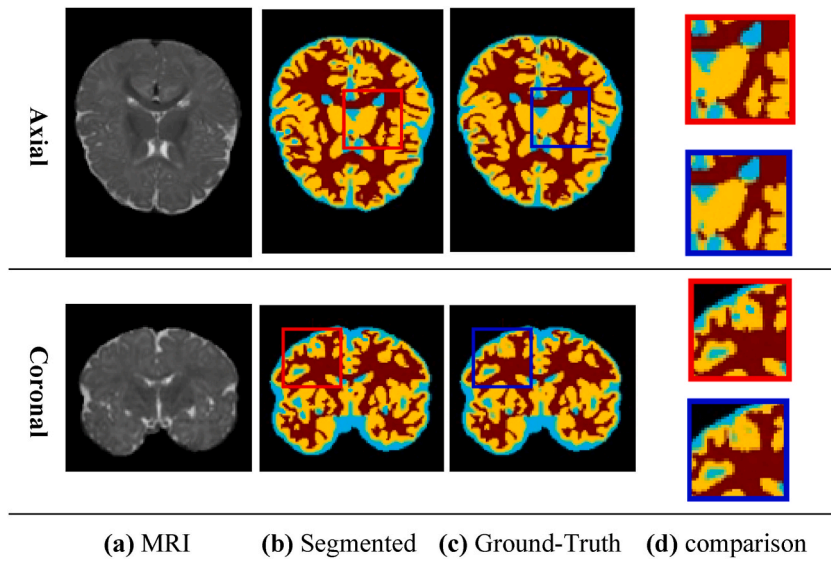**Fig. 7.** Fitness changes in different generations of GA for CNN model optimization.

(a) MRI   **(b)** Segmented   **(c)** Ground-Truth   **(d)** comparison

Fig. 8. Segmentation by the proposed CNN model and its comparison with the background state.
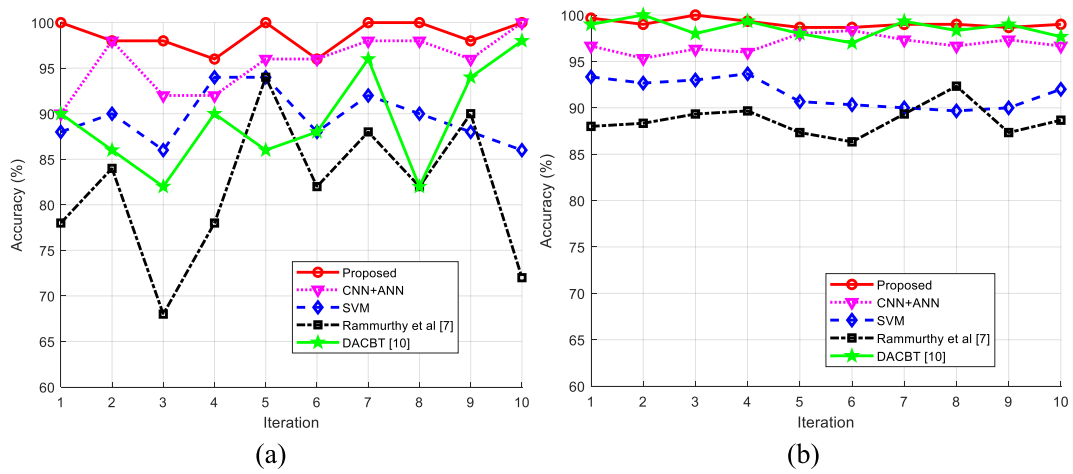

Fig. 9. The accuracy of the proposed method compared to other methods for classifying the images of (a) BRATS2014 and (b) BTD20 during 10 iterations of cross-validation.
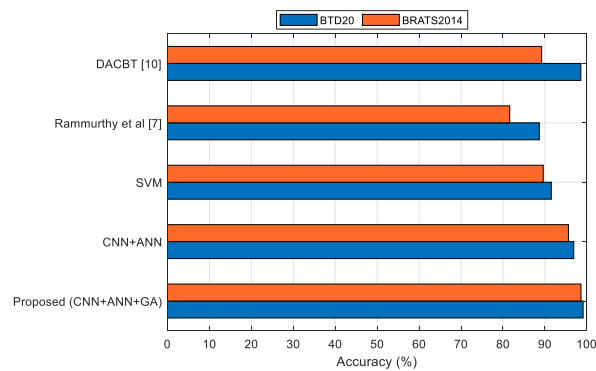

Fig. 10. Accuracy Comparison of different methods in brain tumor classification for BRATS2014 and BTD20.

stated, the efficacy of GA in the optimal configuration of CNN and ANN models is responsible for this enhancement. Overall, the accuracy of classification achieved by various algorithms for BTD20 surpasses that of BRATS2014. Conversely, when contrasting the performance of the proposed approach (CNN + ANN + GA) with the scenario in which GA is not employed to optimize the configuration of CNN and ANN models (CNN + ANN), it becomes evident that the proposed method can enhance the diagnostic accuracy of the BTD20 by a minimum of 2.23 %. Similarly, the BRATS2014 experiences a 3 % increase in accuracy. In addition to validating the efficacy of the optimization algorithm in enhancing the performance of learning models, these results demonstrate that ANN is a more suitable instrument for resolving the BTD problem than alternative classifiers. Subsequently, a minimum enhancement in accuracy of 7.56 % can be attained. As shown in Figs. 9 and 10, the proposed procedure for diagnosing brain lesions has two distinct benefits. Initial, the diagnostic accuracy of the proposed method surpasses that of alternative methods. The assurance of optimal performance in learning models is contingent upon the efficient search in the problem space during the optimization process. Furthermore, when compared to the alternative methods, the proposed technique exhibits a narrower range of accuracy variation. A detection system's restriction of its change range can be regarded as a strength, in conjunction with its high degree of precision. This characteristic serves to demonstrate the dependability of the diagnostic system's outputs. Fig. 11a and b illustrate these conditions in the context of two databases BRATS2014 and BTD20, respectively.

Each box in Fig. 11 illustrates the extent of variation in the algorithm's accuracy over the course of ten iterations of cross-validation. The median value of accuracy throughout the iterations is denoted by the middle circle, while each segment of the box represents one of the quartiles of accuracy change. Additionally, outliers appear as data points outside the frame. The effectiveness of the proposed method in classifying brain tumors in MRI images with greater precision is confirmed by the fact that, according to these diagrams, the proposed method has more condensed boxes positioned at higher levels than other methods.

The confusion matrices of the proposed algorithm for classifying brain tumors in BRATS2014 and BTD20 databases are illustrated in Fig. 12a and b, respectively. Within these matrices, the group of samples devoid of brain tumors is denoted by the number 1, whereas the group of samples harboring brain tumors is denoted by the number 2. The columns of the confusion matrix contain the actual labels of the samples, whereas the rows of each confusion matrix represent the outputs of the learning model (BTD results). By employing this method, the components comprising the primary diameter of each matrix signify the quantity of accurately identified samples belonging to each target class, while the remaining components (designated with the color red) represent the number of classification errors. Fig. 13 also displays the confusion matrix pertaining to the scenario in which GA is not employed for the optimization of the CNN and ANN models. Fig. 13a and b demonstrate the confusion matrices obtained through BRATS2014 and BTD20 datasets, respectively.

The accuracy with which the proposed method identifies each of the target classes is superior to that of the compared state, as shown in Figs. 12 and 13. The proposed method functions nearly identically in separating samples of each class using these matrices. However, overall, the classification error of tumor-containing samples is marginally greater than that of tumor-free samples in both BRATS2014 and BTD20. The findings indicate that the proposed method yields 94 misclassified instances in BTD20 and 22 misclassified instances in BTARS2014 when GA is not utilized. By optimizing the learning models and employing GA, the proposed method effectively decreases the number of misclassified instances to a mere 7 and 27 instances, respectively. Consequently, through the implementation of the optimization strategy in the suggested methodology, we achieved a reduction of over 68 % in the number of classification errors—from 22 to 7.

The received operating characteristics (ROC) curves of various methods for BTD in the BRATS2014 and BTD20 databases are
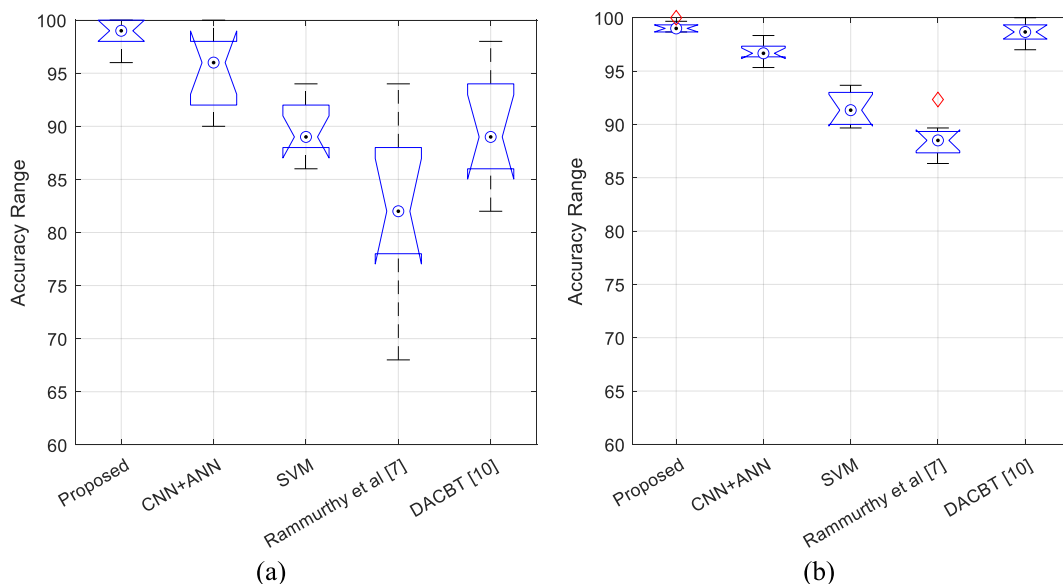

Fig. 11. Box plot of different methods accuracy for two databases (a) BRATS2014 and (b) BTD20 during 10 iterations of cross-validation.
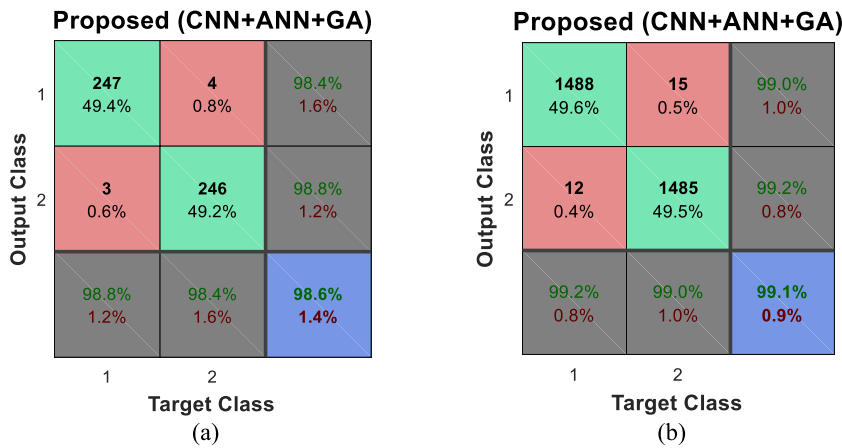
Fig. 12. Confusion matrix of the proposed method for tumor classification in (a) BRATS2014 and (b) BTD20.
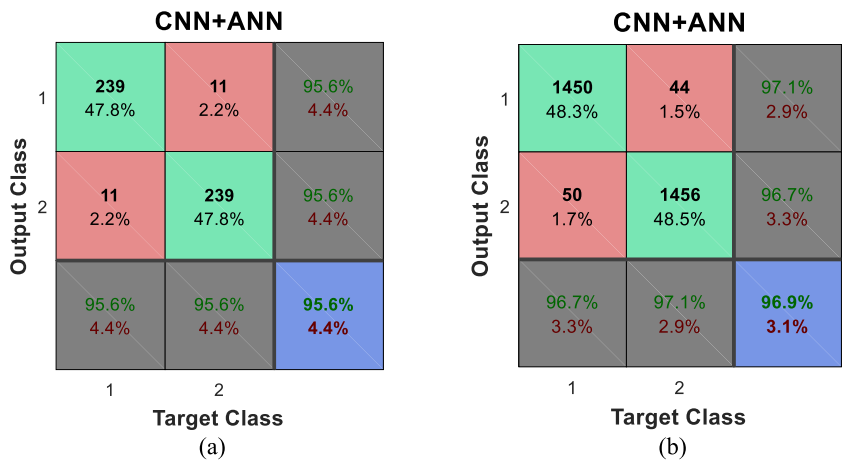

Fig. 13. Confusion matrix in the case of not using GA in (a) BRATS2014 and (b) BTD20.

displayed in Fig. 14a and b, respectively. The values of the true positive rate (TPR) in relation to the false positive rate (FPR) are represented in this curve. The objective of every BTD method is to simultaneously increase TPR and decrease FPR. Consequently, the efficacy of a diagnostic system is enhanced when the ROC curve reaches a greater value.

As illustrated by the graphs in Fig. 14, the proposed method is capable of attaining greater TPR and lesser FPR values for both databases that were tested. These outcomes demonstrate that the proposed procedure outperforms each class individually in terms of BTD. The analysis of the graphs presented in this figure reveals that the compared methods for BRATS2014 and BTD20 exhibit an identical order of performance. Consequently, the proposed method demonstrates the highest level of performance, while the SVM model exhibits the lowest performance. The findings of this study validate that the suggested approach effectively identified brain tumors in the images contained in both databases, leading to increased values of the ROC curve. To enhance the evaluation of the proposed method's efficacy, one may employ metrics such as criteria, precision, recall, and F-Measure. A comparison is made between the efficacy of the proposed method and alternative methods using precision, recall, and F-Measure metrics (see Fig. 15a for BRATS2014 and Fig. 15b for BTD20). Table 1 also contains the numerical results associated with these criteria.

A comparison of precision, recall, and F-Measure values in Table 1 and Fig. 15 indicates that the proposed method may separate samples of each class more effectively. The findings presented herein validate the assertion put forth in this article concerning the efficacy of the optimization approach employed by CNN and ANN models in order to enhance the precision of brain tumor detection in MRI images. Conversely, Table 1's comparison of the proposed method's efficacy to that of its predecessors confirms that this model is capable of classifying brain tumors with greater precision.

5. Conclusion

This paper introduces a novel approach for detecting bone tumor disease (BTD) in MRI images via the use of machine learning and optimization methodologies. The technique under consideration partitions the BTD issue into two distinct sub-problems, namely
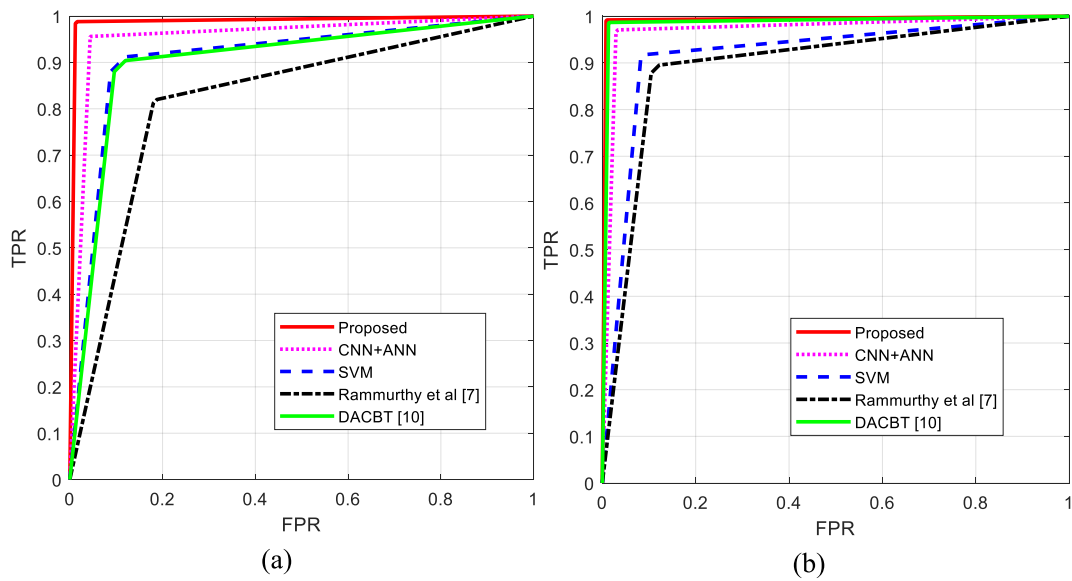
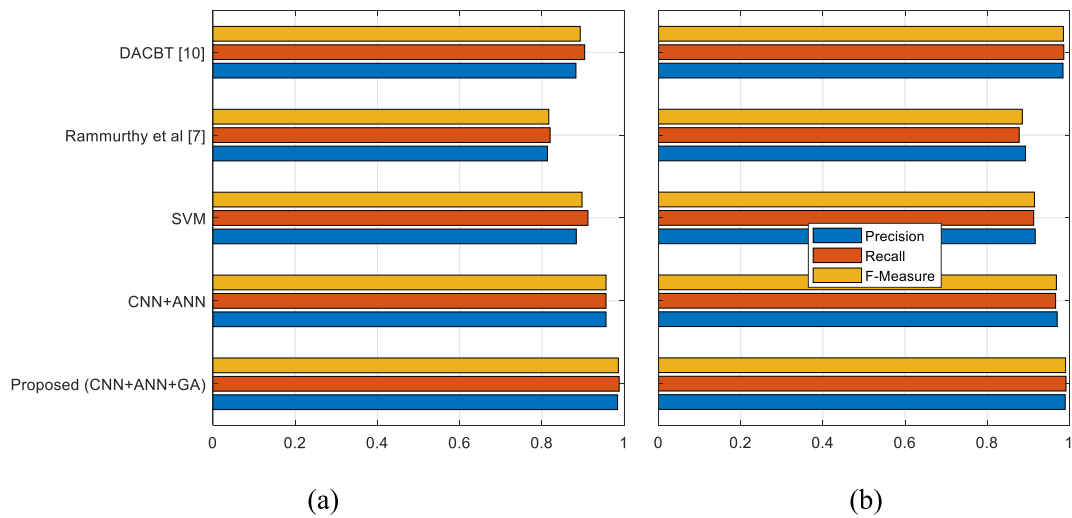**Fig. 14.** ROC curve for tumor classification in (a) BRATS2014 and (b) BTD20.

Fig. 15. Classification quality of brain tumors in (a) BRATS2014 and (b) BTD20.

Table 1
Efficiency comparison of the proposed method to other classification models.

Database	Method	Accuracy	F-measure	Recall	precision
BTD20	Proposed	99.1000	0.9910	0.9920	0.9900
	CNN + ANN	96.8667	0.9686	0.9667	0.9705
	SVM	91.5333	0.9152	0.9133	0.9170
	Rammurthy et al. [7]	88.6667	0.8857	0.8780	0.8935
	DACBT [10]	98.5667	0.9857	0.9867	0.9847
BRATS2014	Proposed	98.6000	0.9860	0.9880	0.9841
	CNN + ANN	95.6000	0.9560	0.9560	0.9560
	SVM	89.6000	0.8976	0.9120	0.8837
	Rammurthy et al. [7]	81.6000	0.8167	0.8200	0.8135
	DACBT [10]	89.2000	0.8933	0.9040	0.8828

"brain segmentation" and "tumor diagnosis". In order to address the initial issue, a Convolutional Neural Network (CNN) with an encoder-decoder architecture is used. The layers of the CNN are equipped with configurable hyperparameters, which are chosen using Genetic Algorithms (GA). This approach aims to optimize the quality of picture segmentation. Conversely, the second sub-problem is addressed by using a pair of Artificial Neural Networks (ANN) and Genetic Algorithms (GA). In this scenario, the selection of the configuration and weight vector for the neural network (NN) is based on the objective of minimizing the training error of the NN. The use of these two tactics sets the present study apart from other investigations, hence enhancing the precision of its diagnosis in comparison to prior methodologies. Furthermore, the suggested methodology employs the MPCA technique for the purpose of extracting features from segmented pictures. The findings of the research indicate a considerable impact of the feature extraction approach on the accuracy of the final diagnosis. By including 190 characteristics, the suggested model may achieve optimal accuracy in accurately diagnosing the lesion. The suggested method's performance was evaluated using two datasets, BRAT2014 and BTD20, and the results were compared to prior comparable studies. The findings obtained from the study demonstrate that the suggested methodology is a reliable approach for the detection of brain tumors using MRI images. The average accuracy achieved in the BRAT2014 and BTD20 datasets was found to be 98.6 % and 99.1 % respectively, surpassing the performance of earlier techniques.

One of the constraints associated with the suggested methodology pertains to the considerable computational intricacy involved in the process of configuring the CNN. However, it is important to acknowledge that the observed time difference is only associated with the setup phase of the Convolutional Neural Network (CNN) model. Given the advancements made in this approach, the computational cost described may be disregarded. However, the temporal disparity may be mitigated by the use of more efficient optimization models or the implementation of parallel processing methods. In future research endeavors, optimization methods may be used to design additional learning models, like deep belief networks and probabilistic neural networks, with the aim of attaining a classification model that is more efficient.

Data availability

All data generated or analysed during this study are included in this published article.

CRediT authorship contribution statement

Jianhong Ye: Project administration, Investigation. **Zhiyong Zhao:** Investigation. **Ehsan Ghafourian:** Investigation. **AmirReza Tajally:** Investigation. **Hamzah Ali Alkhazaleh:** Investigation. **Sangkeum Lee:** Project administration, Investigation.

Declaration of competing interest

The authors declare that they have no known competing financial interests or personal relationships that could have appeared to influence the work reported in this paper.

Acknowledgment

References

[1] S. Das, G.K. Nayak, L. Saba, M. Kalra, J.S. Suri, S. Saxena, An artificial intelligence framework and its bias for brain tumor segmentation: a narrative review, Comput. Biol. Med. (2022) 105273.

[2] R. Ranjbarzadeh, A. Caputo, E.B. Tirkolaee, S.J. Ghoushchi, M. Bendechache, Brain tumor segmentation of MRI images: a comprehensive review on the application of artificial intelligence tools, Comput. Biol. Med. (2022) 106405.

[3] S. Ali, J. Li, Y. Pei, R. Khurram, K.U. Rehman, T. Mahmood, A comprehensive survey on brain tumor diagnosis using deep learning and emerging hybrid techniques with multi-modal MR image, Arch. Comput. Methods Eng. 29 (7) (2022) 4871–4896.

[4] J. Huang, N.A. Shlobin, S.K. Lam, M. DeCuypere, Artificial intelligence applications in pediatric brain tumor imaging: a systematic review, World neurosurgery 157 (2022) 99–105.

[5] M.K. Balwant, A review on convolutional neural networks for brain tumor segmentation: methods, datasets, libraries, and future directions, IRBM (2022).

[6] E. Başaran, A new brain tumor diagnostic model: selection of textural feature extraction algorithms and convolution neural network features with optimization algorithms, Comput. Biol. Med. 148 (2022) 105857.

[7] D. Rammurthy, P.K. Mahesh, Whale Harris hawks optimization-based deep learning classifier for brain tumor detection using MRI images, Journal of King Saud University-Computer and Information Sciences 34 (6) (2022) 3259–3272.

[8] J. Amin, M.A. Anjum, N. Gul, M. Sharif, A secure two-qubit quantum model for segmentation and classification of brain tumor using MRI images based on blockchain, Neural Comput. Appl. 34 (20) (2022) 17315–17328.

[9] S.A. Nawaz, D.M. Khan, S. Qadri, Brain tumor classification based on hybrid optimized multi-features analysis using magnetic resonance imaging dataset, Appl. Artif. Intell. 36 (1) (2022) 2031824.

[10] A.U. Haq, J.P. Li, S. Khan, M.A. Alshara, R.M. Alotaibi, C. Mawuli, DACBT: deep learning approach for classification of brain tumors using MRI data in IoT healthcare environment, Sci. Rep. 12 (1) (2022) 15331.

[11] C.S. Rao, K. Karunakara, Efficient detection and classification of brain tumor using kernel based SVM for MRI, Multimed. Tool. Appl. 81 (5) (2022) 7393–7417.

[12] R. Vankdothu, M.A. Hameed, H. Fatima, A brain tumor identification and classification using deep learning based on CNN-LSTM method, Comput. Electr. Eng. 101 (2022) 107960.

[13] S. Montaha, S. Azam, A.R.H. Rafid, M.Z. Hasan, A. Karim, A. Islam, Timedistributed-cnn-lstm: a hybrid approach combining CNN and lstm to classify brain tumor on 3d MRI scans performing ablation study, IEEE Access 10 (2022) 60039–60059.

[14] M.A. Ottom, H.A. Rahman, I.D. Dinov, Znet: deep learning approach for 2D MRI brain tumor segmentation, IEEE Journal of Translational Engineering in Health and Medicine 10 (2022) 1–8.

[15] M. Aamir, Z. Rahman, Z.A. Dayo, W.A. Abro, M.I. Uddin, I. Khan, Z. Hu, A deep learning approach for brain tumor classification using MRI images, Comput. Electr. Eng. 101 (2022) 108105.

[16] A. Stadlbauer, F. Marhold, S. Oberndorfer, G. Heinz, M. Buchfelder, T.M. Kinfe, A. Meyer-Bäse, Radiophysiomics: brain tumors classification by machine learning and physiological MRI data, Cancers 14 (10) (2022) 2363.

[17] P. Gao, W. Shan, Y. Guo, Y. Wang, R. Sun, J. Cai, Z. Wu, Development and validation of a deep learning model for brain tumor diagnosis and classification using magnetic resonance imaging, JAMA Netw. Open 5 (8) (2022) e2225608.

[18] S. Saeedi, S. Rezayi, H. Keshavarz, S. R. Niakan Kalhori, MRI-based brain tumor detection using convolutional deep learning methods and chosen machine learning techniques, BMC Med. Inf. Decis. Making 23 (1) (2023) 16.

[19] M. Ait Amou, K. Xia, S. Kamhi, M. Mouhafid, A novel MRI diagnosis method for brain tumor classification based on CNN and bayesian optimization, Healthcare 10 (3) (2022, March) 494.

[20] A.B. Abdusalomov, M. Mukhiddinov, T.K. Whangbo, Brain tumor detection based on deep learning approaches and magnetic resonance imaging, Cancers 15 (16) (2023) 4172.

[21] P. Mohan, S. Veerappampalayam Easwaramoorthy, N. Subramani, M. Subramanian, S. Meckanzi, Handcrafted deep-feature-based brain tumor detection and classification using MRI images, Electronics 11 (24) (2022) 4178.

[22] E. Ghafourian, F. Samadifam, H. Fadavian, P. Jerfi Canatalay, A. Tajally, S. Channumsin, An ensemble model for the diagnosis of brain tumors through MRIs, Diagnostics 13 (3) (2023) 561.

[23] M. Kaur, J. Kaur, J. Kaur, Survey of contrast enhancement techniques based on histogram equalization, Int. J. Adv. Comput. Sci. Appl. 2 (7) (2011).

[24] M. Khosravy, N. Gupta, N. Marina, I.K. Sethi, M.R. Asharif, Morphological filters: an inspiration from natural geometrical erosion and dilation, Nature-Inspired Computing and Optimization: Theory and Applications (2017) 349–379.

[25] T. Eelbode, J. Bertels, M. Berman, D. Vandermeulen, F. Maes, R. Bisschops, M.B. Blaschko, Optimization for medical image segmentation: theory and practice when evaluating with dice score or Jaccard index, IEEE Trans. Med. Imag. 39 (11) (2020) 3679–3690.

[26] H. Lu, K.N. Plataniotis, A.N. Venetsanopoulos, MPCA: multilinear principal component analysis of tensor objects, IEEE Trans. Neural Network. 19 (1) (2008) 18–39.

[27] B.H. Menze, A. Jakab, S. Bauer, J. Kalpathy-Cramer, K. Farahani, J. Kirby, K. Van Leemput, The multimodal brain tumor image segmentation benchmark (BRATS), IEEE Trans. Med. Imaging 34 (2014) 1993–2024. BRATS 2014 Dataset. Available online: https://www.smir.ch/BRATS/Start2014. December 2022.

[28] A. Hamada, Br35H brain tumor detection 2020 dataset, Available online: https://www.kaggle.com/ahmedhamada0/brain-tumor-detection, 2020. December 2022.